High-Lift Airfoil Design from the Hodograph

M. J Cohen*
Ben-Gurion University of the Negev, Beersheva, Israel

A practical and general method is described and used to derive particular airfoil sections with the desirable flat roof-top characteristics of some optimum profiles. The method is derived from a solution of the inverse airfoil problem, where the dynamic features required of it by the designer are set in the hodograph plane and the airfoil profile, which will realize those design features obtained by a simple process of numerical integration. All the physical viability criteria are satisfied ab initio and the particular sections calculated exhibit those desirable features by suitably choosing some transformation constants which are fully defined in the hodograph plane. The pressure recovery at the tail end of the upper surface can be helped to develop naturally without separation taking place by making use, if need be, of the process of natural jet injection into the boundary layer at a well-defined station just ahead of an incipient separation point. Some of these so-derived airfoils are described together with their aerodynamic characteristics. The method can also be used to generate high-performance cascade blading for low-speed (incompressible) work, or airfoils, either isolated or in cascades, for use at compressible (subsonic) flow speeds, with little significant structural complexity added.

Introduction

THE purpose of this paper is to present and use a simple hodograph method of designing high-lift airfoils with desirable pressure distributions including flat roof-top airfoils which have deservedly earned them the interest of designers and aerodynamicists alike due to the efficiency of their operation both as high-lift and relatively low-drag aerodynamic devices. The flat roof-top airfoil has been investigated by many authors and Liebeck was one of the first to provide the theoretical and experimental argument for its subsequent adoption as the optimum configuration in the design of efficient airfoil sections. It is not the intention here of giving a history of the development of this class of airfoils; the literature on the subject is fairly extensive and the selection given,[2-8] which is easily obtainable, should be found adequate for those more generally interested. On the other hand, it is the intention to present an alternative analytic method for the synthesis of families of such flat roof-top and other high-lift airfoils using fairly straightforward analytic tools, for which nonseparated flows can be expected. The method obtains from an exact (for the incompressible flow) solution[3] of the inverse problem stated in the hodograph plane from which the required physical profile can be derived. The criteria for profile closure and acceptable physical configurations are satisfied ab initio as it were and the method suggests a straightforward procedure for evolving whole families of such airfoils, each suitable for a specific design task using elementary numerical algorithms easily programmable, and, in many cases, processable on a desk calculator as was done in the example presented here. The method is quite general[2,3] and can be extended to derive cascade airfoil profiles with similarly desirable aerodynamic characteristics and could thus provide an additional powerful tool for the synthesis of efficient turbine (or compressor) blading profiles. Its extension to the whole of the subsonic compressible domain is extant[3] and involves no significant complication in the basic structure of the approach described here. The advantageous characteristics of the particular flat roof-top airfoil sections examined more specifically in this paper are twofold: 1) they all exhibit flat roof-top pressure distributions over *extensive* portions of both upper and lower surfaces and, 2) the *large* pressure differentials between lower and upper surfaces enable a process of high-energy jet injection into any incipiently separating boundary layer to be achieved if needed, by a natural means, at a well-defined point well aft ($> 0.7c$) on the upper surface, where, in some of these profiles, separation may occur due to the sudden onset of the adverse pressure gradient required for pressure recovery. The advantage of the optional approach suggested in this paper, over one based on a process of Stratford[9] pressure recovery appears to be twofold: 1) the airfoil's range of efficient performance on either side of its design point is likely to be more extensive and, 2) the airfoils do not exhibit the long trailing tails on the upper surface (with the concomitant reduction in the lift coefficient) required to enable a full process of Stratford recovery to stay on course all the way to the trailing edge. Finally, the airfoils calculated by this method and presented here, having short "recovery" or trailing sections over their upper surfaces and extensive roof-top sections over both upper and lower surfaces are inherently high-lift and potentially low-drag devices with practically simple and mechanically attractive properties.

Received Oct. 3, 1983; revision received March 28, 1984.

*Guest Professor, Mechanical Engineering Department.

Theoretical Background

For a two-dimensional subsonic (quasi-incompressible) flow about a closed profile, uniform at infinity, there exists a potential function, $W=\phi+i\psi$, such that for every point of the flow, including, of course, those on the profile boundary,

$$\frac{dW}{dz}=\zeta \tag{1}$$

where $z=re^{i\phi}$ and $\zeta=qe^{i\theta}$ are the complex coordinates in the physical and hodograph planes, respectively. Equation (1) shows that the transformation from the physical to the true hodograph planes and vice versa is isogonal. Without loss of generality we shall call the ζ plane, the image in its real axis of the true hodograph plane, the hodograph plane from now on. From Eq. (1) it follows that

$$z=\int \frac{dW}{\zeta} \tag{2}$$

and, therefore, if W is known in any plane ζ_2, derivable by conformal transformation from the hodograph plane ζ, then the profile $z]$ in the physical plane can be derived from a suitable integration around the corresponding boundary in the ζ_2 plane; that is, from Eq. (2),

$$z] = \oint \frac{1}{\zeta} \frac{dW}{d\zeta_2} d\zeta_2 \tag{3}$$

where, in Eq. (3), corresponding points ζ and ζ_2 along the boundary are related by a defined conformal transformation linking those two planes. Any suitable conformal transformation could be used for that purpose and, in particular, those described by a Schwarz-Christoffel relation are of especial interest since they develop an arbitrarily selected polygonal boundary set in a $\ell n\zeta$ plane onto the real axis in the ζ_2 plane. For the sake of analytical simplicity in the working out of the examples and also because of their proven aerodynamic efficiency, application of the method presented will be restricted to families of airfoils with so-called "flat roof-top" velocity distributions. These are made up of linked velocity segments which are either of constant speed or of constant inclination. Thus, if a ℓn-hodograph plane $\zeta_1 = \ell n\zeta$ is interposed between the ζ and ζ_2 planes, the boundary profiles in the ζ_1 plane, for any of these families of airfoils, are now all polygonal with corner angles in multiples of $\pi/2$, thus exhibiting the characteristic flat roof-top feature (Figs. 1-3). The "unperturbed" conditions at infinity in the physical plane are represented by a doublet singularity within the polygonal boundary In particular, if the unperturbed stream velocity vector is taken as unity, conditions at infinity in the physical plane flow, in the presence of an airfoil, will be represented by a doublet at the origin in the ζ_1 plane, with axis normal to the real axis. In addition, there is a vortex superimposed at that doublet location whose strength Γ is equal to the strength of the circulation around the airfoil in the physical plane. The polygonal boundary within which the doublet-vortex flow is contained in the ζ_1 plane can now be transformed to the flow in the upper half of a ζ_2 plane by a suitable Schwarz-Christoffel transformation

$$\frac{d\zeta_1}{d\zeta_2} = \text{const.}\,(\zeta_2 - 1)^{\alpha_1/\pi - 1}(\zeta_2 + 1)^{\alpha_2/\pi - 1}(\zeta_2 - k_1)^{\alpha_3/\pi - 1}$$

$$\times (\zeta_2 - k_2)^{\alpha_4/\pi - 1}(\quad) \tag{4}$$

where α_1, α_2, etc. are the internal angles at the corners of the boundary polygon in the ζ_1 plane and will all be, for the cases worked here, multiples of $\pi/2$. The actual form of these transformations is given in each case in Figs. 1-3. Generally, the strength $(\mu)_{\zeta_1}$ of the doublet (at $\zeta_1 = \zeta_{10} = 0$) in the ζ_1 plane is, of course, affected by the transformation to the ζ_2 plane, so that the corresponding strength of the doublet at $\zeta_2 = \zeta_{20}$ in the ζ_2 plane is:

$$(\mu)_{\zeta_2} = (\mu)_{\zeta_1}\left(\frac{d\zeta_2}{d\zeta_1}\right)_{\zeta_2 = \zeta_{20}} \tag{5}$$

with the vortex strength Γ remaining unaffected by the transformation.

The flow from and to a doublet-vortex singularity system at $\zeta_2 = \zeta_{20}$, in the upper half of the ζ_2 plane, i.e., with the real

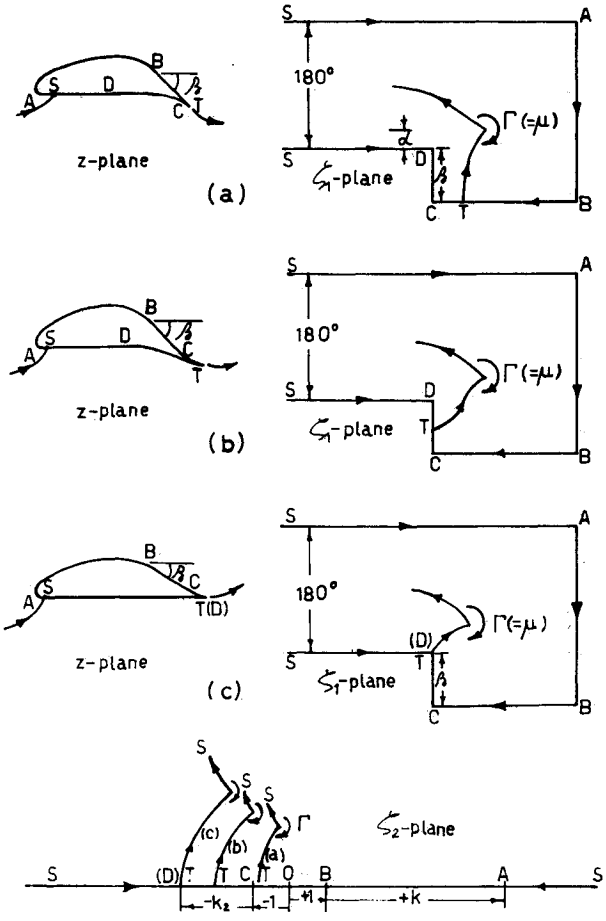

Fig. 1 First family of high-lift airfoils, $\frac{d\zeta_1}{d\zeta_2} = \frac{-\sqrt{\zeta_2 + k_2}}{\sqrt{(\zeta_2^2 - 1)(\zeta_2 - k_1)}}$

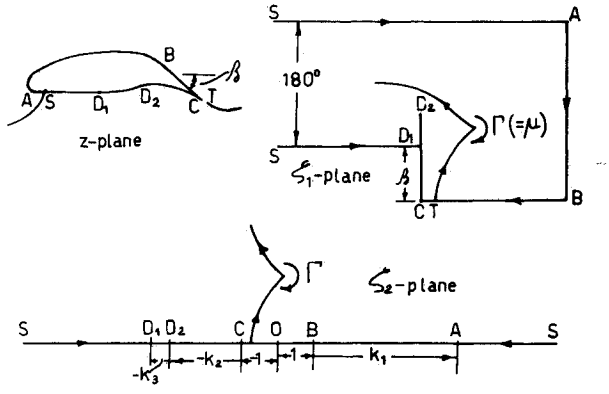

Fig. 2 Second family of high-lift airfoils, $\frac{d\zeta_1}{d\zeta_2} = \frac{-\sqrt{(\zeta_2 + k_3)}}{\sqrt{(\zeta_2^2 - 1)(\zeta_2 - k_1)(\zeta_2 + k_2)}}$

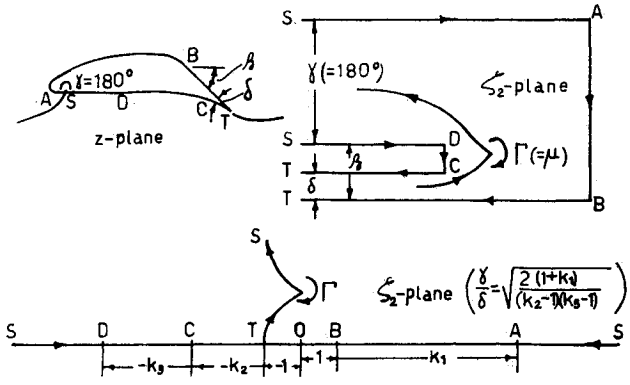

Fig. 3 Third family of high-lift airfoils, $\frac{d\zeta_1}{d\zeta_2} = \frac{-\gamma\sqrt{(\zeta_2 + k_2)(\zeta_2 + k_3)}}{\pi(\zeta_2 + 1)\sqrt{(\zeta_2 - 1)(\zeta_2 - k_1)}}$

axis as a boundary, is given by the potential function

$$W(\zeta_2)=\frac{1}{2\pi}\left[\frac{(\mu)_{\zeta_2}}{\zeta_2-\zeta_{20}}+i\Gamma\ell n(\zeta_2-\zeta_{20})\right]+\text{image in real axis} \quad (6)$$

In Eq (6) only one of μ and Γ is arbitrary (that arbitrariness is reflected in the arbitrariness of the scale of the derived profile), the other must be expressed in terms of it by a subsidiary condition which, as will be shown in the next paragraph, is provided by the condition of profile closure in the physical plane. Since the velocity vector selected as standard dynamic quantity is the unit (scalar) vector in the $\bar{\zeta}$ plane, all the other parameters determining the boundary in the hodograph plane are referred to it and can be selected by the designer to suit his purpose, and, subject to the transformation in Eq (4), the potential function $W(\zeta_2)$ and, therefore, $dW/d\zeta_2$ are completely known To perform the integration (Eq 3) along the real axis in the ζ_2 plane, which yields, by integrative construction the corresponding airfoil profile in the physical plane, one needs the appropriate $\bar{\zeta}$ corresponding to each point ζ_2 along the integration path For those sections of the real axis in the ζ_2 plane corresponding to constant stream inclination θ_r segments of the airfoil profile,

$$\frac{1}{\bar{\zeta}}=e^{-\zeta_1}=\frac{1}{q}e^{i\theta} \quad (7a)$$

and for the sections corresponding to constant stream speed q_r, flat roof top, segments of the airfoil profile,

$$\frac{1}{\bar{\zeta}}=e^{-\zeta_1}=\frac{1}{q_r}e^{i\theta} \quad (7b)$$

with the $\zeta_1=f(\zeta_2)$ required in the integrand obtained from Eq (4) by integration along the (real axis) boundary in the ζ_2 plane. The process of airfoil synthesis defined by Eq (3) is thus one of numerical piecemeal integration around a contour in the ζ_2 plane, which is the (closed) boundary of the whole of its upper half The starting point for this integration could be any convenient point along the real axis of the ζ_2 plane proceeding anticlockwise to "+" infinity and back from "-" infinity to the original starting point, via the circle at infinity The corresponding path in the physical plane z] will describe the countour of the desired airfoil The full form of the integral [Eq (3)] can be written by the use of Eq (6):

$$z]=\frac{1}{2\pi}\oint e^{-\zeta_1}\left[i\Gamma\left(\frac{1}{\zeta_2-\zeta_{20}}-\frac{1}{\zeta_2-\bar{\zeta}_{20}}\right)-\kappa\left(\frac{e^{i\nu}}{(\zeta_2-\zeta_{20})^2}+\frac{e^{-i\nu}}{(\zeta_2-\bar{\zeta}_{20})^2}\right)\right]d\zeta_2 \quad (8)$$

with ζ_2 real ($=\xi_2$) here, and where $(\mu)_{\zeta_2}=\kappa e^{i\nu}$, $\zeta_{20}=\xi_{20}+i\eta_{20}$ and ζ_1 is related to ζ_2 by the integrated form of Eq (4)

Figures 1 3 show three families of flat roof top airfoils together with their attendant ζ_1 plane configurations

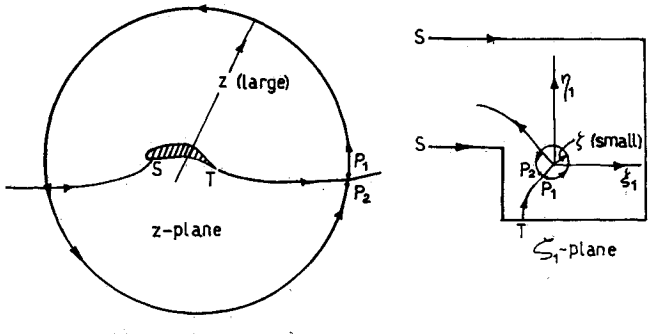

Fig 4 Contour integration path for profile closure

Analytical Development

There are three subsidiary conditions that must be satisfied in order to obtain acceptable physical airfoil profiles:

1) The profiles must close in the physical plane

2) The stagnation points must be physically viable; that is, a forward stagnation point *near* the leading edge of the profile and a rear stagnation point *at* the trailing edge of the profile if the trailing edge is not cusped or a dividing streamline leaving the trailing edge smoothly if it is

3) The profile must not cross over itself in the process of its synthesis The first condition establishes the principle of continuity of the main flow The second ensures the satisfaction of the Kutta Zhukovski condition at the trailing edge, and the third, in part a restatement of the first, also ensures the generation of a physically valid profile

Condition of Profile Closure

Referring to Fig. 4, it is clear that the airfoil profile will close exactly provided the dividing streamline leaves an un split trailing edge of the closed profile at T to proceed as a single streamline to infinity downstream. If a contour integration of dz is taken around a large circle (in the limit, the infinite circle) starting just above the lip of the dividing streamline to a point just below it at the end of the contour, then the condition for profile closure is:

$$\oint dz=0 \quad (9)$$

This condition translates both in the ζ_1 and ζ_2 planes to an integration around an infinitesimally small circle around the doublet vortex singularity representing the flow conditions at infinity in those planes; that is, condition (9) becomes the contour integral (identical to Eq. (8), but with a different path of integration),

$$\oint dz=\oint\frac{1}{\bar{\zeta}}\frac{dW}{d\zeta_2}d\zeta_2=\oint e^{-\zeta_1}\frac{dW}{d\zeta_2}d\zeta_2=0 \quad (10)$$

in the ζ_2 plane, where the contour integration is taken around a small circle in the ζ_2 plane surrounding the singularity at $\zeta_2=\zeta_{20}$ Let the doublet strength (at $\zeta_1=0$) in the ζ_1 plane be

$$(\mu)_{\zeta_1}=\lim_{\substack{m\to\infty\\ \delta\epsilon\to 0}}[(m\delta\epsilon)e^{-i\pi/2}]\neq -i\mu \quad (11)$$

where μ is the modulus of the doublet strength in the ζ_1 plane

$$[\text{i e}\,,\ \mu=\lim_{\substack{m\to\infty\\ \delta\epsilon\to 0}}(m\ \delta\epsilon)],$$

where m is the strength of either source of sink comprising the doublet and $\delta\epsilon$ is their angular separation (the doublet axis

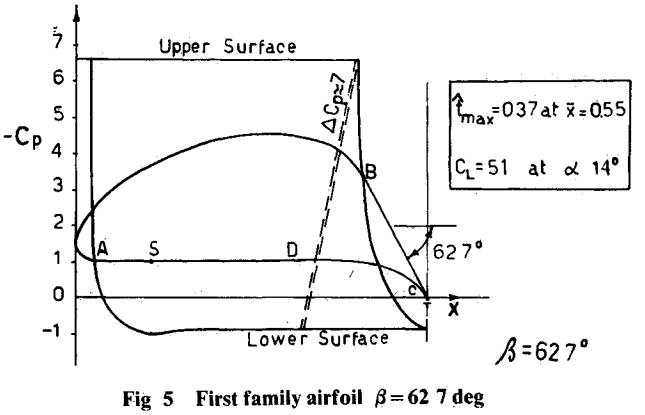

Fig 5 First family airfoil $\beta=62\ 7$ deg

length in the ζ_1 plane). Then, from Eq (5), the strength of the doublet at $\zeta_2=\zeta_{20}$ in the ζ_2 plane is

$$(\mu)_{\zeta_2}=-i\mu\left(\frac{d\zeta_2}{d\zeta_1}\right)_{\zeta_2=\zeta_{20}}=\kappa e^{i\nu} \tag{12}$$

But for corresponding regions in the neighborhood of the doublet vortex singularities in the ζ_1 and ζ_2 planes, the transformation function must take theTaylor form:

$$\zeta_1=(\zeta_2-\zeta_{20})\left(\frac{d\zeta_1}{d\zeta_2}\right)_{\zeta_2=\zeta_{20}}+0[(\zeta_2-\zeta_{20})^2]$$

Hence, for small ζ_1,

$$e^{-\zeta_1}\doteq 1-\zeta_1\doteq 1-(\zeta_2-\zeta_{20})\left(\frac{d\zeta_1}{d\zeta_2}\right)_{\zeta_2=\zeta_{20}}$$

and the integral, Eq (10), now reduces, using Eq (8) for the different contour examined here to

$$\oint dz=\frac{1}{2\pi}\left\{i\Gamma\oint\frac{d\zeta_2}{(\zeta_2-\zeta_{20})}+\kappa e^{i\nu}\left(\frac{d\zeta_1}{d\zeta_2}\right)_{\zeta_2=\zeta_{20}}\oint\frac{d\zeta_2}{(\zeta_2-\zeta_{20})}\right\}=0 \tag{13}$$

that is

$$-\Gamma+i\kappa e^{i\nu}\left(\frac{d\zeta_1}{d\zeta_2}\right)_{\zeta_2=\zeta_{20}}=0$$

or by Eq (12),

$$\Gamma-\mu=0$$

Hence, the condition for airfoil profile closure is equivalent to the following relationship between the strengths (scalar) of the superimposed vortex and doublet singularities in the ζ_1 plane:

$$\Gamma=\mu \tag{14}$$

This simple relationship yields an interesting physical in terpretation which will be described in the sequel The in tegration process that will ensure profile closure is thus from Eq (8),

$$\bar{z}]=i\oint e^{-\zeta_1}\left\{\left[\frac{1}{\xi_2-\zeta_{20}}-\frac{1}{\xi_2-\bar{\zeta}_{20}}\right]+\frac{\left(\frac{d\zeta_2}{d\zeta_1}\right)_{\zeta_{20}}}{(\xi_2-\zeta_{20})^2}-\frac{\left(\frac{d\zeta_2}{d\zeta_1}\right)_{\bar{\zeta}_{20}}}{(\xi_2-\bar{\zeta}_{20})^2}\right\}d\xi_2 \tag{15}$$

where $\bar{z}=2\pi z/\Gamma$ and $e^{-\zeta_1}$, corresponding to points ξ_2 on the real axis in the ζ_2 plane, is given by the appropriate expression [Eqs (7a or 7b)] and has either constant argument (for those parts of the real axis corresponding to the constant velocity inclination segments of the boundary in the ζ_1 plane) or constant modulus (for those parts of the real axis corresponding to constant speed segments of the boundary in the ζ_1 plane)

Choice of the Stagnation Points

From a consideration of the "forward" stagnation point at S in Figs 1 3, it is clear that the corresponding stagnation point in the ζ_2 plane must lie at infinity. Thus one of the two stagnation points on the real axis in that plane is at infinity and the other at some suitable position on that axis That latter position determines the kind of airfoil (flat, single reflex double reflex) with cusped trailing edge to be designed (Figs 1 and 2) For airfoils with finite trailing edge angle, Fig 3, the second stagnation point on the real axis must be at point T in that plane,, which is one of the corner points of the polygon in the ζ_1 plane

Families of Airfoils with Cusped Trailing Edges

The forward stagnation point S lies at infinity in the ζ_2 plane In that plane the velocity distribution along the real axis is, from Eqs (6), (12) and (14),

$$\frac{d\bar{W}}{d\zeta_2}=-2\{\xi^2{}_2(\eta_{20}+\bar{\kappa}\cos\nu)-2\xi_2(\xi_{20}\eta_{20}+\bar{\kappa}\cos\nu\xi_{20}+\bar{\kappa}\sin\nu\eta_{20})+[\eta_{20}(\xi_{20}^2+\eta_{20}^2)+2\bar{\kappa}\sin\nu\eta_{20}\xi_{20}+\bar{\kappa}\cos\nu(\xi_{20}^2-\eta_{20}^2)]\}/[\xi_2^2-2\xi_2\xi_{20}+(\xi_{20}^2+\eta_{20}^2)]^2 \tag{16}$$

where $\bar{W}=2\pi W/\Gamma$, $\bar{\kappa}=\kappa/\Gamma$, and $\zeta_2=\xi_2+i\eta_2$

Hence, for just one stagnation point on the real axis, we get from Eq (16) the condition

$$\eta_{20}+\bar{\kappa}\cos\nu=0 \tag{17}$$

where

$$\bar{\kappa}=\text{mod}\left(\frac{d\zeta_2}{d\zeta_1}\right)_{\zeta_2=\zeta_{20}}\quad\text{and}\quad\nu=\left\{\arg\left(\frac{d\zeta_2}{d\zeta_1}\right)_{\zeta_2=\zeta_{20}}-\frac{\pi}{2}\right\}$$

from Eq (12)

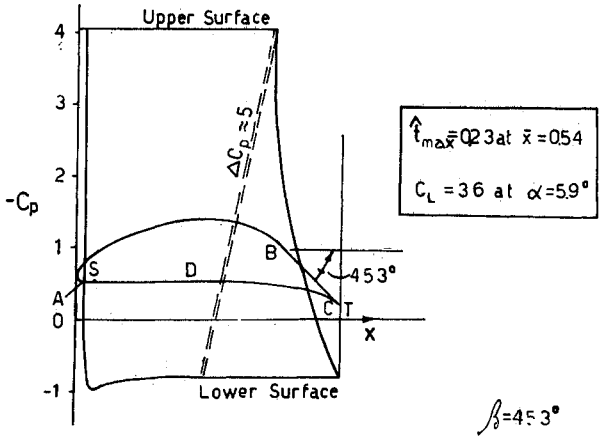

Fig 6 First family airfoil $\beta=45.3$ deg.

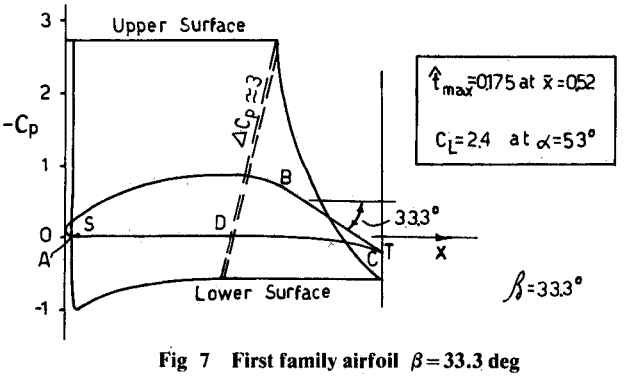

Fig 7 First family airfoil $\beta=33.3$ deg

Once the family of desired cusped trailing-edge airfoils is selected, the appropriate $d\zeta_2/d\zeta_1$ is known (see Figs 1 and 2) and Eq (17) then determines a locus of η_{20} values corresponding to a set of so far arbitrary ξ_{20} values, all yielding acceptable forward stagnation points The choice of ξ_{20} is not, however, wholly arbitrary for ξ_{20} in fact, also fixes (with its attendant η_{20}) the position of the other stagnation point at $\xi_2 = \xi_{2S}$; that is, at T, on the real axis of the ζ_2 plane, which for airfoils of the first family, should lie between D and O, that is, $-k_2 < \xi_{2S} < 0$ The position of this stagnation point at T in the ζ_2 plane corresponding to the trailing edge at T in the physical plane can easily be obtained from Eq (16) as:

$$\xi_{2S} = \xi_{20} - \frac{\eta_{20}}{\tan\nu} \tag{18}$$

after making use of relation (17) Generally any ξ_{20} which yields by Eq (18) a value of $-k_2 < \xi_{2S} < 0$ is acceptable and will ensure that the airfoil boundary in the physical plane does not cross over itself There is an infinite number of airfoils with cusped trailing edges in each family depending on (a) the set $\{k_1 \quad k_2, \quad\}$ chosen, which is dominant in determining the airfoil geometry, thickness ratio, incidence, and, hence, its eventual C_L; and the ξ_{20} selected for each such set, which is less so If, without loss in profile efficiency, T is chosen to coincide with C in the ζ_1 plane, the second stagnation point ξ_{2S} in the ζ_2 plane lies at $\xi_2 = -1$, and Eq (18) then yields

$$\frac{\eta_{20}}{\tan\nu} - \xi_{20} = 1 \tag{19}$$

and Eqs (17) and (19) now give for ξ_{20}

$$\xi_{20} = \bar{\kappa}\left(\frac{1}{\sin\nu} - \sin\nu\right) - 1 \tag{20}$$

Since $\bar{\kappa}$ and ν are both functions of η_{20} and ζ_{20} [see Eq (12)], Eqs. (17) and (20) are two simultaneous nonlinear equations for determining the two unknowns (ξ_{20} and η_{20}) which define the singularity position on the hodograph planes A solution of these equations can be quite easily obtained on a programmable desk calculator (in a time on the order of 5 min on a TI59), for each of the set $\{k_1 \quad k_2 \quad\}$ chosen to define a particular cusped airfoil in that family Three high lift airfoils of this first family have been so designed and are drawn in Figs. 5 7, together with their pressure distributions at the stated design angle of attack

Family of Airfoils with Finite Angled Trailing Edges

Figure 3 describes another family of flat roof top airfoils but with finite trailing edge angles For these airfoils Eq (17) is still valid for the forward stagnation points, but there is an additional relation [similar to Eq (18)] fixing the rear stagnation point at the trailing edge T, which, in this case, is that point on the real axis of the ζ_2 plane corresponding to the appropriate "corner" dscribing the trailing edge flow in the ζ_2 plane; that is, a second point at infinity (at T) in the ζ_1 plane If the point T in the ζ_2 plane is at $\zeta_2 = -k_s$, this second relation is, from Eq (18)

$$\xi_{20} - \frac{\eta_{20}}{\tan\nu} = -k_s \tag{21}$$

which, together with Eq (17), determines the two unknowns ξ_{20} and η_{20} uniquely This can be performed easily on a desk calculator as in the previous case

Worked Examples and Discussion

On the basis of the foregoing, the procedure for the development of a flat roof-top airfoil profile of the type described is as follows:

1) A set of $\{k_1 \quad k_2, \quad\}$ is chosen This apart from an arbitrary scale constant determines $d\zeta_1/d\zeta_2$ completely (See Figs. 1 3)

2) ζ_1 values on the profile boundary, corresponding to a suitable string of ζ_2 values along the real axis in the ζ_2 plane stretching from $-\infty$ to $+\infty$ is obtained from the preceding by numerical integration from some suitable point, say, ξ_{2S} on that axis This yields the correspondence required in Eq (8) between ζ_1 and ξ_2:

$$\zeta_1 - \zeta_{1s} = \int_{\xi_{2S}}^{\xi_2} \frac{d\zeta_1}{d\zeta_2} d\zeta_2 \tag{22}$$

$\Delta\zeta_1$ lengths along constant speed segments of the boundary will be wholly imaginary, whereas $\Delta\zeta_1$ lengths along constant inclination segments of the boundary will be wholly real

3) The coordinates ($\xi_{20} \quad \eta_{20}$) fixing the position (ζ_{20}) of the doublet vortex singularity in the ζ_2 plane, corresponding to the particular set of $\{k_1 \quad k_2, \quad\}$ chosen, is determined by solving simultaneously the two equations (17) and (18)

4) ζ_{10}, the position of the doublet-vortex singularity in the ζ_1 plane, representing conditions at infinity in the physical plane can now be obtained from

$$\Delta\zeta_1 = \int_{\xi_{20}}^{\zeta_{20}} \frac{d\zeta_1}{d\zeta_2} d\zeta_2$$

the integral being performed along a path parallel to the imaginary axis of the ζ_2 plane. This yields the real and imaginary increments $\Delta\xi_1$ and $\Delta\eta_1$, from the (known) point on the ζ_1 plane boundary corresponding to the point ξ_{20} on the real axis of the ζ_2 plane For the airfoils of the first family developed in this paper, these increments are:

$$\Delta\xi_1 = K\begin{pmatrix}\sin\\ -\cos\end{pmatrix}\theta$$
$$\Delta\eta_1 = K\begin{pmatrix}\cos\\ \sin\end{pmatrix}\theta \tag{23}$$

where

$$K = 4\sqrt{\frac{(\xi_{20}-k_2)^2+\eta_{20}^2}{[(\xi_{20}^2-\eta_{20}^2-1)^2+4\eta_{20}^2\xi_{20}^2][(\xi_{20}-k_1)^2+\eta_{20}^2]}}$$

and

$$\theta = \frac{1}{2}\left[\tan^{-1}\frac{\eta_{20}}{\xi_{20}-k_1} + \tan^{-1}\frac{\eta_{20}}{\xi_{20}-1} + \tan^{-1}\frac{\eta_{20}}{\xi_{20}+1} - \tan^{-1}\frac{\eta_{20}}{\xi_{20}-k_2}\right]$$

using, in Eq (23), the upper and lower trigonometric functions, depending on whether $|\xi_{20}| < 1$ or $\xi_{20} > 1$, respectively

5) ζ_{20} and ζ_{10} being now known, $W(\zeta_2)$ is known and the integral Eq (15) can be performed numerically A good starting point for the integral would be the forward stagnation point S

Worked Examples

Three airfoils of the first family were calculated by the above procedure as examples of the use of the present method for the design of a certain type (flat roof-top) of high lift airfoil:

Airfoil A: $k_1 = 10$, $k_2 = -5$, yielding:

$q_M = 2\ 744$, $q_m = 0\ 296$, $\beta = 62\ 7$ deg, $\hat{t} = 0\ 37$,

$C_L = 5.1$ at $\alpha = 14\ 0$ deg

with the resulting pressure distribution shown in Fig 5

Airfoil B: $k_1=20, k_2=-5$, yielding:

$q_M=2\ 241, \quad q_m=0\ 466, \quad \beta=45\ 3$ deg, $\quad \hat{t}=0.23,$

$C_L=3.6$ at $\alpha=5\ 9$ deg

with the resulting pressure distribution shown in Fig 6.

Airfoil C: $k_1=40, k_2=-5$ yielding:

$q_M=1\ 928, \quad q_m=0\ 636, \quad \beta=33\ 3$ deg, $\quad \hat{t}=0\ 175,$

$C_L=2\ 4$ at $\alpha=5\ 3$ deg

with the resulting pressure distribution shown in Fig 7. In the above q_M and q_m are the maximum and minimum constant speeds on the flat roof-top segments of upper and lower surfaces, respectively, and $\hat{t}$ is the thickness ratio; that is, $\hat{t}=t_{\max}/c$. These three airfoils of the first family with cusped trailing edges have three important characteristics:

1) Extensive regions ($>0.7c$) of constant high suction on the upper surface and less extensive but significant stretches of constant relatively high pressures on the lower surface

2) A maximum thickness positioned aft to the midchord

3) A significant $0\{(0.2c)\}$ extent of the rear upper surface sloping down at constant inclination β, right down to the trailing edge.

The first two characteristics are important and justify the expectation of the airfoils being high-lift and low-drag sections The third characteristic suggests that, in the three cases presented, the rear part of the airfoil performs aerodynamically in a fashion similar to that of a deflected flap in a conventional airfoil and that, hence, at the higher values of β, separation may be expected to occur at a point just downstream of B, with or without the formation of a separation bubble.

Boundary Layer Control at Separation Point

Depending mainly on the Reynolds number of the flow, the boundary layer at B on the upper surface can be either still laminar or, having transmitted to turbulence earlier at a point upstream of B, to be already turbulent at B In either case, because of the onset of a sudden adverse pressure gradient at B, flow separation is likely to occur, when it does, just downstream of that point, unless a procedure, yielding gradual (Stratford) pressure recovery over the tail end of the upper surface of the airfoil, were incorporated in the technique of airfoil genesis used, such as has been done by Liebeck et al.,[4,6] or, where the need may arise (as at the higher values of β), re energizing the boundary layer at that point by jet blowing By the provision of a well-defined point at, or shortly beyond which, separation must, when it does, occur first and of an extensive, large, and constant pressure dif ferential between upper and lower surfaces across the airfoil chord, this design method provides, when needed, a natural means of boundary-layer blowing by use of these stable and well-defined, high-pressure differentials Thus, a suitably designed duct leading from any convenient inlet area on the lower surface between D and $C(T)$ to a slot at point B, on the upper surface, discharging a relatively high-energy jet tangentially over BT, would completely inhibit the onset of separation provided the blowing coefficient C_μ is adequate Reference 10 provides a simple empirically based criterion backed by observations of boundary layer control ex periments at NASA, NPL, and ONERA, for the achievement of this aim Thus, if

$$C_\mu \equiv \frac{\rho U_j^2 h}{\frac{1}{2}\rho_\infty U_\infty^2 c} \geq 0\ 015 \tan\beta \tag{24}$$

where β is the "flap" deflection angle, U_j the jet blowing speed, and h the slot width at B, c being the airfoil chord, separation can be expected to be wholly avoided In terms of airfoil characteristics, C_μ can be written as

$$C_\mu = 2(C_{\rho_{lm}} - C_{k_{uM}})(1-k^2)\bar{h} \tag{25}$$

where k is the slot outlet to duct inlet area ratio, whose square will be a small quantity and $\bar{h}=h/c$ A comparison of Eqs (24) and (25) gives the slot width required at B to avoid separation as

$$\bar{h} \geq \frac{0\ 015 \tan\beta}{2(C_{\rho_{lm}} - C_{\rho_{uM}})} \tag{26}$$

Since $2(C_{\rho_{lm}} - C_{\rho_{uM}})/\tan\beta$ is of order 10, in the three cases studied, any h larger than say 0 002 (allowing for duct losses) would be adequate for the purpose, a reasonable and technically practicable value It may also be noted that, although not worked out here, where only airfoils with rounded leading edges have been examined, airfoils with sharp leading edges (leading edge angle $\gamma<\pi$) can be obtained in an identical fashion by the present method But these are perhaps more suitable as cascade-blading profiles and hence more relevant to a very similar procedure applicable for the design of such airfoils in cascades, not described explicitly here For these airfoils, which would be suitable as efficient profiles for compressor or turbine blading, the flow within a polygonal boundary in the ζ_1 plane would be that from a source to a sink with associated circulations It is to the concept of an isolated airfoil, represented by a doublet-vortex combination in the hodograph plane, as the limiting case of a normal cascade of airfoils of infinite pitch, represented by a coalescing source-sink pair in the hodograph plane, that an interesting interpretation can be put on the relationship, Eq (4). In compressible flow, with the fluid density ρ variable, that relationship takes the form $\Gamma=\mu/\rho_\infty$, as dimensional considerations or the definitions of source-sink strength vs vortex strength would show. If, in addition, the unperturbed velocity at infinity were taken not as the standard (unit) speed, but were denoted by U_∞, then Eq (4) could be rewritten for the compressible (subsonic case) as

$$\rho_\infty U_\infty \Gamma = \mu U_\infty$$

that is, by Eq (11),

$$\rho_\infty U_\infty \Gamma = \lim_{\substack{m\to\infty \\ \delta\epsilon\to 0}} [mU_\infty \delta\epsilon]$$

The right-hand side represents the change in momentum normal to the direction of U_∞, of the infinite mass of fluid flowing every second past an isolated airfoil; that is, it is equivalent to the lift experienced by the airfoil and $L=\rho_\infty U_\infty \Gamma$ at all (subsonic) speeds and acts normal to the direction of the unperturbed speed

Conclusions

The ease with which the three airfoils were derived, using a relatively rudimentary desk calculator, suggests that a straightforward computational procedure could be initiated with modest time outlay on any of the larger computers in common use today to synthesize rapidly sets of such high lift airfoils covering a useful range of possible angles of attack and thickness ratios For the airfoil families computed here, for example, a particular set $\{k_1 \quad k_2 \quad \cdot\}$ describing a hodograph configuration, would result in a single high lift flat roof top airfoil with the particular angle of attack, thickness ratio, and β angle corresponding to that con figuration

The method of isolated airfoil design presented provides a means of obtaining high lift sections, with extensive peripheral areas with laminar wing characteristics As such, the associated frictional drag should be correspondingly low This drag and especially the attendant form drag can be expected to be reduced, where needed, by a natural (i.e , involving no supporting mechanical device) in built boun dary layer blowing capability which is one of the features of the design method, and which could be used to inhibit any flow separation tendency over any sharply "sloping away" aft section of the upper surface The considerable "thickness ratio" range and type variety achievable suggest that lists of ready made computed profiles for families of such airfoils could be useful in enabling a suitable choice to be made of high lift profiles for a variety of purposes, such as propeller sections and glider and other wing sections

References

[1]Lighthill M J A New Method of Two Dimensional Aerodynamic Design, ARC R&M 2112 1945

[2]Legendre R , ' Trace des Ailettes pour Fluides a Densite Con stante,' Bulletin de l'Association Technique Maritime et Aeronautique Vol 43 1939.

[3]Cohen M J Hodograph Design Method for Compressible Flow Problems *Journal of Applied Mechanics* Vol 29, 1962 pp 533 548

[4]Liebeck, R H and Ormsbee, A I Optimization of Airfoils for Maximum Lift *Journal of Aircraft* Vol 7 Sept Oct 1970 pp 409 415

[5]Weber, J , The Calculation of the Pressure Distribution on the Surface of Thick Cambered Wings and the Design of Wings with Given Pressure Distribution ARC R&M 3026 1955

[6]Liebeck, R H and Smith A M O A Class of Airfoils Designed for High Lift Without Separation in Incompressible Flow *Journal of Aircraft* Vol 10, Oct 1973 pp 610 617

[7]Strand T , Exact Method of Designing Airfoils with Given Velocity Distributions in Incompressible Flow ' *Journal of Aircraft*, Vol 10 Nov 1973 pp 651 659

[8]Smith A M O 'High Lift Aerodynamics *Journal of Aircraft* Vol 12 June 1975 pp 501 530

[9]Stratford B S The Prediction of Separation of the Turbulent Boundary Layer *Journal of Fluid Mechanics* Vol 5 1959, pp 1 16

[10]Poisson Quinton Ph and Le Page L French Research on Control of Boundary Layer and Circulation *Boundary Layer & Flow Control* Vol 1, edited by G V Lachmann Pergamon Press New York 1961 pp 21 73